THE AMERICAN SOCIETY OF MECHANICAL ENGINEERS
345 E. 47th St., New York, N.Y. 10017

94-GT-90

A CFD ASSESSMENT OF ENTRANCE AREA DISTRIBUTIONS IN A CENTRIFUGAL COMPRESSOR VANELESS DIFFUSER

James M. Sorokes
Dresser-Rand Turbo-Products Division
Olean, New York

ABSTRACT

The paper presents the results of a CFD study that assessed the various area distributions typically found in impeller / diffuser transitions in industrial centrifugal compressor stages. Results for two transition area schedules are compared. The findings agree with recently published data and suggest that problems exist in some standard configurations that could lead to rotating stall in the downstream vaneless diffuser.

NOMENCLATURE

b_2	-	impeller tip width
b_3	-	diffuser entrance width
I	-	grid planes in the blade to blade direction
J	-	grid planes in the inlet to exit (streamwise) direction
K	-	grid planes in the hub to shroud direction
LE	-	leading edge
PS	-	pressure surface
SS	-	suction surface
TE	-	trailing edge
ϕ	-	Flow coefficient = $Q/((\pi^2/4)ND_2^3)$ where: Q = flow in ACFM (m^3/min); N = operating speed in RPM; and D_2 = impeller diameter is feet (m)

INTRODUCTION

Though numerous novel vaned diffusers have been developed, the majority of industrial centrifugal compressors still employ vaneless diffusers. The wide range achievable with vaneless diffusers is desirable to customers who must often operate their compressors over a variety of flow conditions. Much has been written about the sizing of vaneless diffusers to achieve acceptable performance and avoid stall phenomena. In addition, many works have addressed overall area distributions through the diffuser; promoting such concepts as constant area, parallel wall, or other area schedules. However, the transition area between the impeller exit to diffuser entrance has not received as much attention and this region is equally critical to effective stage performance. This paper cites publications (ref. 5, 6, and 7) that suggest the crucial role played by the diffuser entrance area distribution in high pressure centrifugal compressor applications. The authors; Kobayashi, Fukushima, Nishida, and Takagi; tested various entrance configurations and drew conclusions regarding their relative effectiveness with regard to stall margin and elimination of subsynchronous vibration. Their efforts prompted the CFD study described in this paper.

The CFD study analyzed two of the configurations tested by the earlier researchers. These results are compared for both a low and a high flow coefficient impeller. The purpose was to determine if the CFD code could detect any flow phenomena in the diffuser entrance region that might influence the stall margin, diffuser performance, and vibration characteristics.

The Dawes code, BTOB3D, (Dawes 1988) was used for this study despite its suspected limitations in calculating discontinuous flow passages. Comments regarding the assumptions / compromises in the analyses are included.

BACKGROUND

From 1988 through 1991, Kobayashi, Fukushima, Nishida, and Takagi published three reports (ref. 5, 6, & 7) presenting results of their studies on rotating stall in centrifugal compressors. The first paper (reference 7) dealt with the effects of diffuser width on rotating stall. The authors conducted a series of tests using three impeller configurations of different flow coefficients with varying diffuser widths. As expected, as the vaneless diffuser width was increased, the onset of rotating stall occurred at higher flow rates for all three wheels. The authors compared their findings on critical flow angle for stall onset to predictions

Presented at the International Gas Turbine and Aeroengine Congress and Exposition
The Hague, Netherlands – June 13–16, 1994

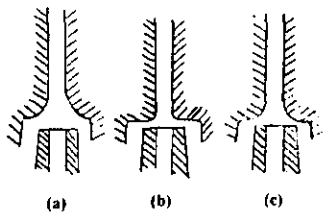

FIGURE 1 – DIFFUSER ENTRANCE GEOMETRIES TESTED BY KOBAYASHI ET AL. (REF. 5)

derived using the Senoo method (Senoo 1978). They found that they encountered rotating stall at lower flow angles than those predicted by the Senoo method. They further discovered that as the ratio of diffuser width to impeller exit radius was decreased, the discrepancy between predicted and actual onset increased. They concluded from this initial work that the ratio of diffuser width to impeller exit width could be used to correct the Senoo method and improve the prediction for critical angle. However, they also noted that diffuser inlet shape (or area schedule) could also influence stall onset.

The above observation led to their second study published in 1990 (reference 5). In this work, Kobayashi et al. tested the same impellers used in their earlier study. However, in this instance, they concentrated on the area distribution into the vaneless diffuser (see figure 1). They found that the flow rate at which rotating stall occurred was sensitive to the impeller/diffuser transition geometry. This was particularly true on the lower flow coefficient stages while of less significance on the higher flow stage. They found that they could extend the stall margin on the narrowest impeller by modifying the diffuser inlet shape while holding the remainder of the passage at constant width. Diffuser inlet variation did not show the same trend with the largest impeller; stall occurred at the same flow regardless of inlet shape. Still, their findings suggested that it was insufficient to treat only the parallel portion of the vaneless diffuser width when striving to avoid rotating stall. Therefore, Kobayashi et al. proposed further modifications to the Senoo method to account for the diffuser entrance effect.

Their final publication (reference 6) studied the effectiveness of using low solidity vaned diffusers (LSD) to extend the stall margin. The LSD proved very beneficial in extending the usable operating range of the stage; suppressing rotating stall better than any of the vaneless diffuser configurations. Numerous others have reported on the benefits of the LSD, therefore, no additional comments will be included here. However, the results of the diffuser inlet shape study were somewhat surprising. That is, the authors had demonstrated that rotating stall could arise despite having sized a vaneless diffuser width using accepted criteria.

There are numerous criteria published to determine the passage width, critical flow angle, radius ratio, and other vaneless

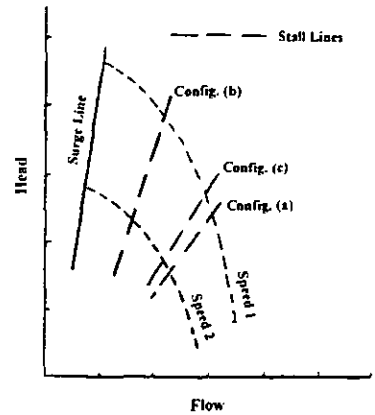

FIGURE 2 – STALL MARGINS FOR VARIOUS DIFFUSER INLET GEOMETRIES (REF. 5)

diffuser attributes necessary to avoid vaneless diffuser rotating stall. Most, if not all, can be found in references 4 and 10. These criteria have proven to be quite successful and are widely applied. However, compressor vendors experience unexpected occurrences of rotating stall which manifest themselves as subsynchronous rotor vibrations. The vibration frequencies encountered fall within the typical range for vaneless diffuser rotating stall; despite having diffusers which conform to the classic criteria for critical flow angle. Therefore, other factors must contribute to the stall phenomenon. Based on the recent work by Kobayashi, et al., one of these factors may be the diffuser inlet profile.

There are differing opinions regarding the most effective impeller/diffuser transition. Some designers feel it necessary to provide excess area above the impeller exit, similar to that seen in figure 1(a) or 1(c). Therefore, the diffuser entrance width is made wider than the impeller exit width. They believe this oversizing insures that the impeller exit is not obstructed by the vaneless diffuser wall; the theory being that such an obstruction could cause shaft vibration due to the impeller/diffuser interaction. Others believe that the best arrangement is to size the diffuser entrance width equal to the impeller exit width as in figure 1(b). These designers theorize that the excess area is detrimental to stage stall margin; providing a potential source for stall and, therefore, causing subsynchronous vibration. The works of Kobayashi et al. seem to support the latter opinion.

Again, figure 1 shows the three diffuser inlet configurations tested by Kobayashi et al. They found that geometry 1(a) yielded the poorest stall margin for the low flow coefficient stage. Configuration 1(c) was only slightly better while the stall margin improved significantly for style 1(b). The test results for the three area schedules are sketched in figure 2. Clearly, excess area above the low flow coefficient impeller had a detrimental effect on stall margin. In an attempt to discern any flowfield anomolies that may be contributing to the difference in stall characteristics, CFD studies were conducted on

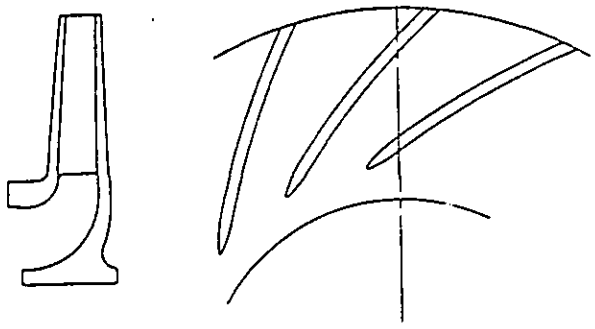

FIGURE 3 – LOW FLOW IMPELLER

configurations similar to 1(b) and 1(c). Case 1(a) was not analyzed as the area increase was believed to be too severe.

ANALYSIS APPROACH

To assess the various impeller/diffuser transitions, models were developed and analyzed using the Dawes code, BTOB3D (Dawes 1988). This code is intended for axisymmetric turbomachinery applications (e.g., impellers, diffusers, return channels, rotor blades, stator vanes). The users need only grid one passage of the component and the code assumes symmetry for the other passages. The version used in this study was modified to perform a shrouded impeller analysis. That is, the shroud surface rotates with the blades and hub. Of course, the shroud surface does not rotates beyond the impeller trailing edge.

The BTOB3D solution is based on the time-dependent Reynolds-averaged Navier-Stokes equations and employs the Baldwin-Lomax turbulence model. Note, it is not the intent of this paper to describe the governing equations or algorithms used in the Dawes code. Instead, this paper concentrates on an unusual application of BTOB3D. For those interested, reference 2 provides a description of the equations and/or algorithms involved.

The calculation domain consisted of an axial inlet section and a full impeller, followed by the vaneless passage. The impeller used in cases #1 and #2 is a low flow coefficient design (ϕ =.030), similar to the wheel used by Kobayashi et al. (ref. 5, 6, & 7). The impeller meridional and axial configuration are shown in figure 3.

In generating the calculation mesh, the inlet to the impeller was defined by an axial projection of the impeller inlet hub and shroud diameters. The vaneless diffuser passage width was reduced to a level consistent with the classic criteria for avoidance of rotating stall (Jansen 1964, Senoo 1978). Further, the diffuser was extended to a radius ratio of 1.4 to insure that the calculation boundary was far enough removed from the impeller/diffuser transition. Finally, to insure that adequate

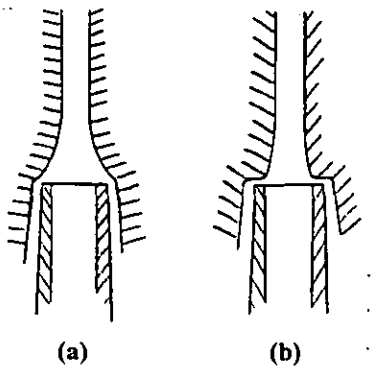

FIGURE 4 – DIFFUSER ENTRANCE GEOMETRIES USED IN THE CFD ANALYSES

detail was obtained, the grid spacing was reduced in the impeller-diffuser transition.

The transition region between the impeller exit and the pinched width was varied as shown in figure 4. Configurations (a) and (b) are very similar to two of the styles used by Kobayashi et al. – figure 1(c) & 1(b), respectively – with one exception. While testing the effects of inlet shape, Kobayashi et al. set the parallel segment of their diffuser width equal to the impeller tip width. As noted, in this study, the diffuser width was pinched to conform with classic criteria (Jansen 1964, Senoo 1978) for avoiding rotating stall.

COMPROMISES IN THE COMPUTATIONAL MODEL

Before discussing the CFD results, it is important to note the analytical compromises involved in the solutions described in this paper. The code is sensitive to the computational grid. Therefore, the step changes in the wall profile, simulating the sudden expansion above the impeller exit, may induce inaccuracies in the solutions.

Second, BTOB3D assumes symmetry and, therefore, does not require a full 360° grid. While advantageous in the modeling effort, the assumed symmetry compromises the user's ability to analyze the mixing which occurs at the impeller exit.

The third and most significant compromise concerns the treatment of the flow at the impeller exit. Typically in shrouded wheels, a small amount of flow recycles over the cover back to the impeller inlet. Unfortunately, BTOB3D ignores this recirculation flow, assuming that all of the flow which exits the impeller moves on into the diffuser. Obviously, this is not rigorously correct.

Despite the acknowledged limitations, BTOB3D was used for a variety of reasons. First, the code has gained wide acceptance in the turbomachinery world. Numerous papers have been published showing good agreement between BTOB3D analyses and measured data (e.g. references 1 and 8). While none of the published works included a discontinuous flow passage, it was

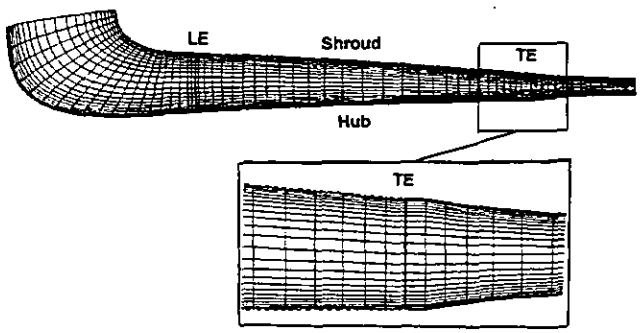

FIGURE 5 – GRID USED FOR CASE #1

felt that a small step would not present a significant challenge to the code. Second, there were no suggestions in the open literature that the Dawes code is inappropriate for this study. Therefore, the analyses were completed to determine if BTOB3D, despite its shortcomings, could identify any flow trends that might promote diffuser instability. Third, as will be seen, the BTOB3D results agree with the findings of Kobayashi et al.;showing differences in the flow profiles that may explain the variation in tested stall margin. Fourth, it was not obvious that other CFD codes would offer any better solutions. Even if a more appropriate code did exist, the computational power required to simultaneously analyze the inlet, impeller, diffuser, and cover recirculation flow would be prohibitive for the industrial compressor designer. Fifth, since the cases herein were all performed using the same assumptions, the comparisons of qualitative results are still valid. In addition, the solutions were all converged to the same mass flow error and residue levels to insure consistency between the individual cases. Still, in deference to the possible inaccuracies, no quantitative results (velocity, entropy, pressure magnitudes) will be discussed. Finally and most significant, when this work was completed, BTOB3D was the only CFD code available to this author.

PLOT FORMATS

Results are presented in the following formats:

- Entropy Contour Plots - These plots portray regions of entropy generation. By noting such, the observer can identify regions which contribute to higher disorder of the flowfield. Obviously, such disorder contributes to higher losses and may indicate the presence of a stall or separation zones. The plots are shown as planes perpendicular to the direction of flow, often referred to as normal or "J" planes.
- Pressure Contour Plots - These plots provide a three-dimensional representation of the static pressure at various normal planes ("J" planes). Regions of depressed static pressure can quickly be identified.
- Pseudo (Zero Mass) Particle Traces - These visuals trace the path that a zero mass particle would take if released in the flow stream. Helpful for flow visualization, these plots are very popular to the CFD analyst. Regions of swirl, reverse flow, and normal throughflow are obvious to even an untrained eye. Note, particle traces are typically a postprocessor function. The postprocessor uses the analytical results to determine on an element by element basis how a particle will move through the flow passage.

The plots presented in this paper were generated using two CFD postprocessing systems: PLOT3D available through NASA and POSTDAWES from Concepts, ETI.

CASE #1 – DIFFUSER INLET WIDTH EQUAL TO IMPELLER EXIT WIDTH

The calculation grid for case #1 is shown in figure 5. In this configuration, the diffuser entrance width was set equal to the impeller exit width. Therefore, there is no excess area above the impeller. This transition is similar to configuration 1(b) tested by Kobayashi et al. except that the diffuser passage reduces to approximately 60% of the impeller tip width. Recall, Kobayashi et al. found that this configuration yielded the largest tested stall margin for the low flow coefficient stage (see figure 2).

The entropy levels for various normal planes ("J" planes) are shown in figures 6 through 9, corresponding to radius ratios (radius to plane divided by impeller exit radius) of 1.0, 1.007, 1.023, and 1.057, respectively. Note the small high entropy zones that appear near the suction surface in figure 6. These reflect the wakes formed in the impeller that are shed into the diffuser. The wakes are a combination of secondary flow from the impeller passage and the blade wakes themselves; i.e., disturbances caused by the trailing end of the blades. The entropy zones remain visible in successive "J" planes but the level of variation diminishes as the flow progresses into the pinched diffuser (note figure 9).

The diffuser entrance pressure profile is given in figure 10. There is little to note in this profile. In general, the pressure distribution looks quite uniform and does not suggest any pressure disturbances that might cause unbalanced forces on the rotor.

A pseudo-particle trace for case #1 can be seen in figure 11. Only traces near the suction surface are shown and the view is from the diffuser looking back toward the impeller exit. The flow appears very well-behaved as the streaklines travel only in the flow-wise direction.

In short, the CFD results do not indicate any problems with this transition geometry, showing none of flow anomalies (swirling or reverse flows) that might indicate the potential for stall or poor performance. Therefore, the CFD results support the findings of Kobayashi et al. that this configuration should exhibit good stall margin.

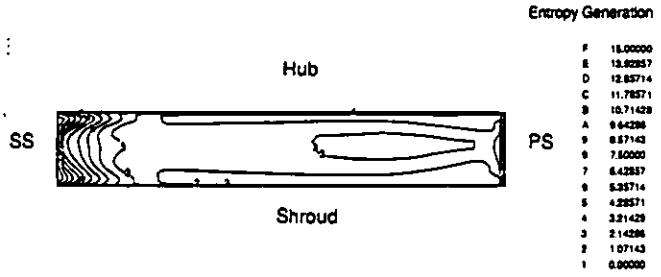

FIGURE 6 – ENTROPY CONTOURS AT IMPELLER EXIT PLANE

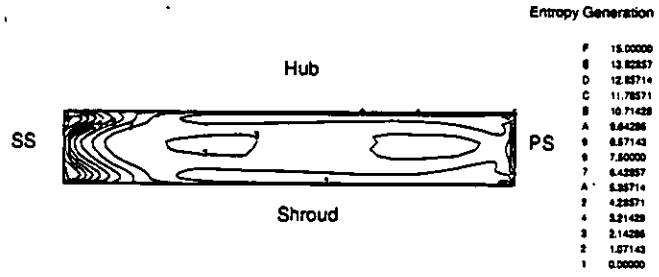

FIGURE 7 – ENTROPY CONTOUR AT RADIUS RATIO = 1.007

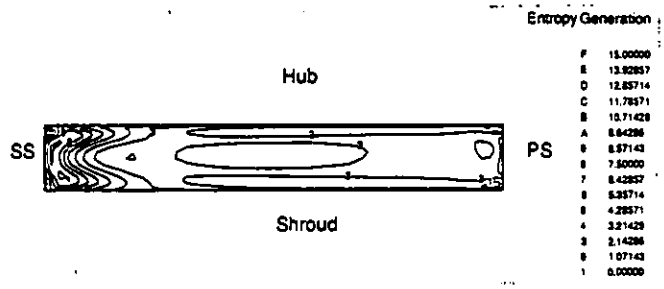

FIGURE 8 – ENTROPY CONTOUR AT RADIUS RATIO = 1.023

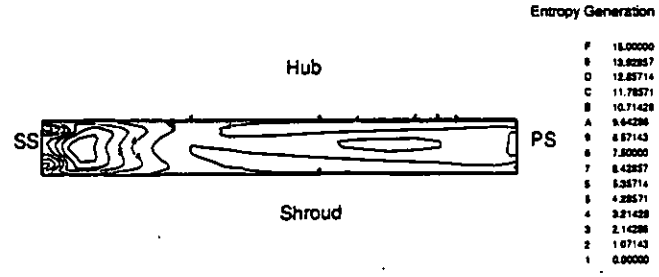

FIGURE 9 – ENTROPY CONTOUR AT RADIUS RATIO = 1.057

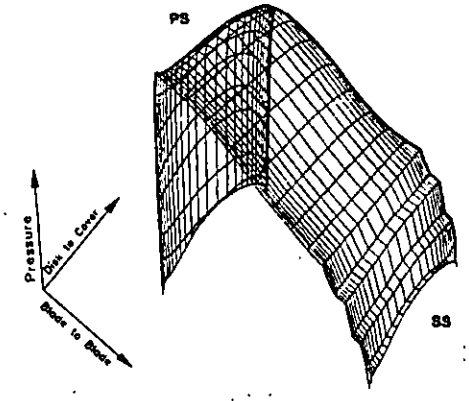

FIGURE 10 – DIFFUSER ENTRANCE STATIC PRESSURE DISTRIBUTION

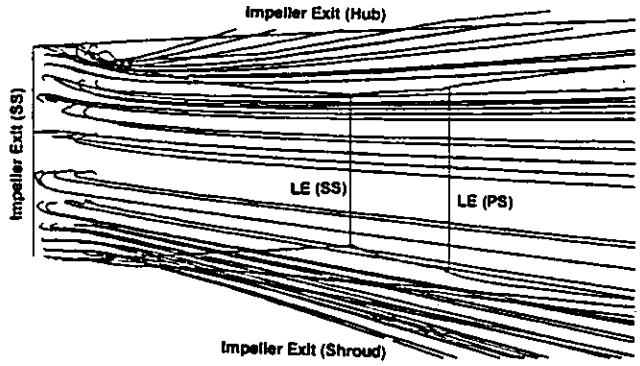

FIGURE 11 – PSEUDO-PARTICLE TRACE

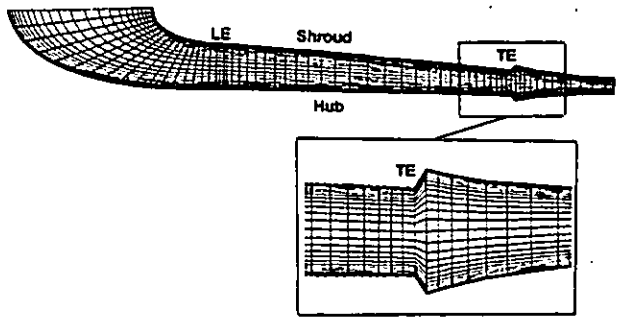

FIGURE 12 – GRID FOR CASE #2

CASE #2 – DIFFUSER INLET WIDTH EQUAL TO 140% OF IMPELLER EXIT WIDTH

The grid used for case #2 is shown in figure 12. In this instance, the diffuser inlet width was set at 140% of the impeller's exit; approximating configuration 1(c) described by Kobayashi et al. This transition reflects the geometry prescribed by those wishing to avoid diffuser wall interference with the impeller exit flow.

The entropy contours are shown in figures 13 through 16. The entropy distribution at the impeller exit plane (figure 13) appears very similar to that from case #1 (figure 6). However,

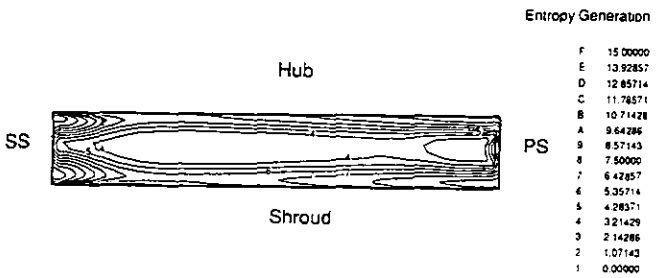

FIGURE 13 – ENTROPY CONTOURS AT IMPELLER EXIT PLANE

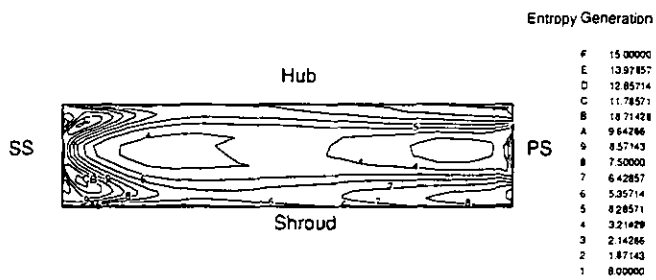

FIGURE 14 – ENTROPY CONTOUR AT RADIUS RATIO = 1.007

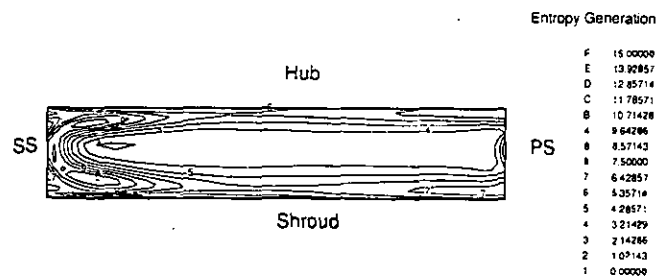

FIGURE 15 – ENTROPY CONTOUR AT RADIUS RATIO = 1.023

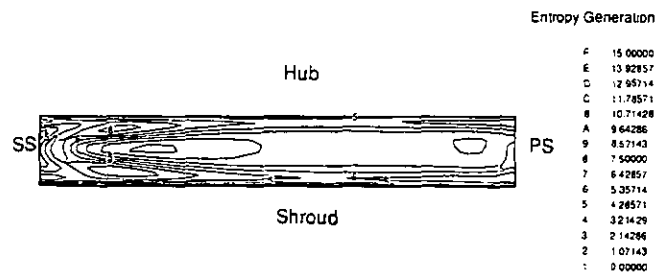

FIGURE 16 – ENTROPY CONTOUR AT RADIUS RATIO = 1.057

there are subtle differences. Additional entropy islands can be seen along the hub and cover surfaces, suggesting that the excess area is influencing the flow in the impeller; i.e., backflow.

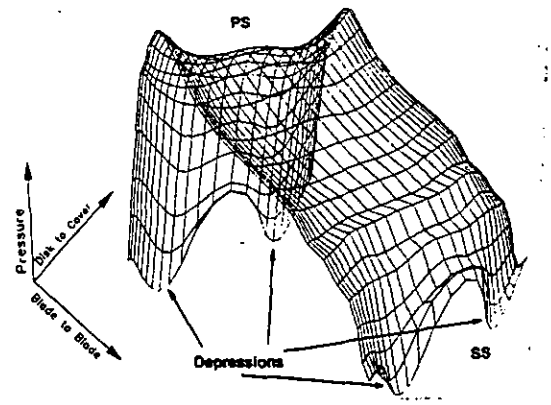

FIGURE 17 – DIFFUSER ENTRANCE STATIC PRESSURE DISTRIBUTION

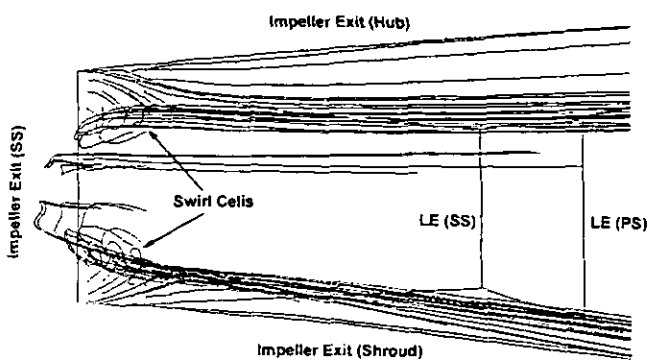

FIGURE 18 – PSEUDO PARTICLE TRACE

At the first calculation plane within the diffuser, there are significant differences between this and the earlier case. In figure 14, the wake regions near the suction surface are much larger than for case #1 (figure 7); evidenced by the larger increased entropy regions along the hub and shroud surfaces. Obviously, secondary flows occupy a larger portion of the flow passage as a consequence of the excess area above the impeller exit. Note that as the flow progresses further into the diffuser (figure 15 & 16), two high entropy islands are visible; one along each wall. In the earlier case, these islands had begun to dissipate at these calculation planes (figure 8 & 9). In this case, the islands remain fairly large. In general, these results suggest that the flow in the case #2 transition configuration is more disturbed.

A review of the diffuser inlet static pressure distribution shows significant differences between case #2 and case #1 results. In case #2, large regions of depressed static pressure are visible at the diffuser entrance plane (figure 17). Compare this distorted distribution to smooth contour seen in figure 10. Obviously, such non-uniformity in pressure can detrimentally affect diffuser performance and, if sufficiently large, can contribute to unbalanced forces that cause rotor excitation/vibrations.

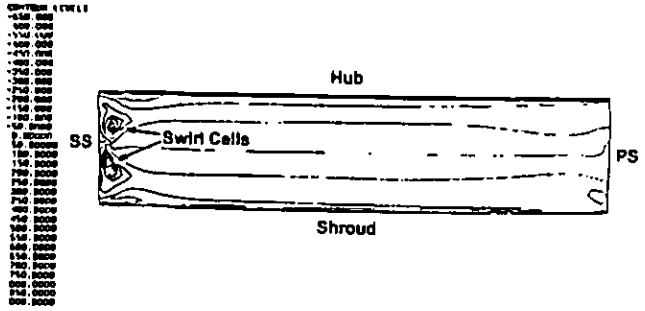

FIGURE 19 – SWIRL PLOT CASE #2

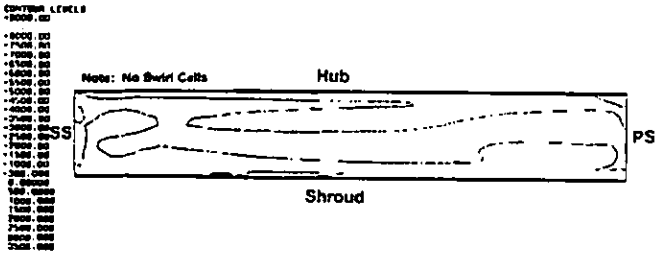

FIGURE 20 – SWIRL PLOT CASE #1

The flow disturbances become clear in the pseudo-particle traces for case #2 (see figure 18). Again, as viewed looking back into the impeller exit, there are two obvious swirls (as noted) in the flow near the suction surface; one near the shroud wall and one near the hub. The swirl cells appear to rotate in opposite directions and are the result of viscous forces acting upon the wake flow in the recess area.

Review of the swirl contour plot for this case (figure 19) confirms that the cells do counter-rotate. The swirl velocities are negative along the hub and positive along the shroud. Note, no such cells appear in the swirl plot for the case #1 (figure 20).

Given the above observations, it is clear that the excess area above the impeller exit promotes disturbances in the diffuser passage. These disturbances, if not detrimental in and of themselves, likely cause further problematic effects in the diffuser; i.e., rotating stall. Clearly, case #1 does not exhibit the same flow anomalies as seen in case #2. Therefore, based on these CFD results, one might have anticipated the results obtained by Kobayashi et al.; i.e., that removal of the excess area on the low flow coefficient stage would lead to improved stall margin.

A point must be made before proceeding further. The author anticipated that including excess area above the impeller would result in flow anomolies. It was felt that low momentum fluid (wakes) from the impeller would coalesce in the excess area and potentially lead to premature diffuser stall. Therefore, it was not surprising that the CFD code predicted swirling secondary flow along the hub and shroud surfaces in the sudden expansion. In fact, since the code predicted the expected trends, the author gained confidence in the code's ability to analyze the odd impeller - diffuser transition geometries.

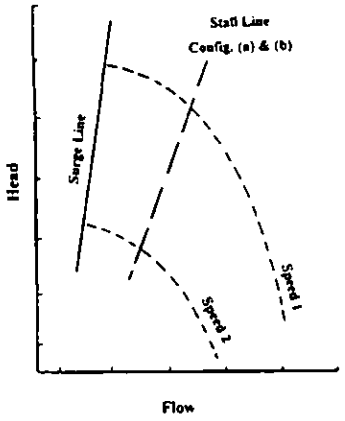

FIGURE 21 – TEST RESULT FOR HIGH FLOW IMPELLER (REF. 5)

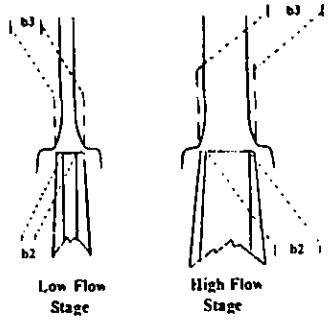

FIGURE 22 – DIFFUSER ENTRANCE GEOMETRIES WITH b3 - b2 = CONSTANT

CASE #3 – AREA EXPANSION FOLLOWING A HIGH FLOW IMPELLER

Nishida et al. showed that the excess area did not seem to have any influence on the larger flow impeller (see figure 21). This suggests that the amount of area expansion relative to the impeller's exit width must play a role in determining what detrimental effects the area will have. Centrifugal designers tend to apply a fixed increase in passage width regardless of impeller tip width. Consequently, using this approach, a smaller impeller will suffer more than a larger one (see figure 22). That is, flow from a smaller impeller 'sees' a larger percentage increase in area from its tip width to the diffuser entrance width. Likewise, the level of radial versus tangential velocity will influence the sensitivity to the extra area. One would expect that an impeller having a large exit radial velocity will be less sensitive to a sudden expansion in area.

To investigate these points, two CFD analyses was performed using a high flow coefficient impeller (ϕ = 0.150). Runs were done with and without the sudden expansion over the impeller exit. For the case including the expansion, the increase in diffuser entrance width was the same amount used in case #2; i.e., b3-b2 for case #3 equals b3-b2 for case #2. The area was

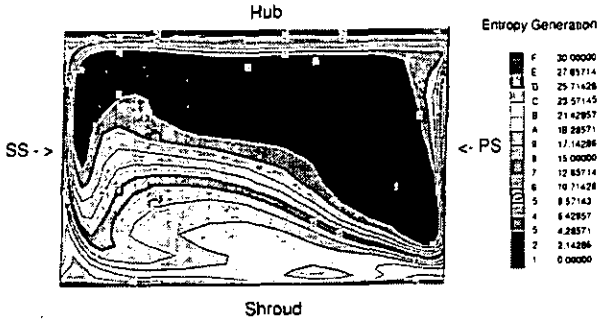

FIGURE 23 – ENTROPY CONTOUR DIFFUSER ENTRANCE WITH SUDDEN EXPANSION

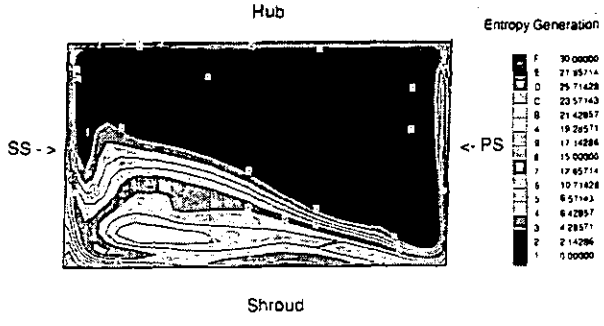

FIGURE 24 – ENTROPY CONTOUR DIFFUSER ENTRANCE WITHOUT SUDDEN EXPANSION

then decreased symmetrically from both walls to a final passage width equal to the impeller tip width. Note, this impeller also has a more radial exit flow angle than the impeller used in cases 1 and 2; that is, the ratio of radial to tangential velocity is higher.

The diffuser entrance entropy contours for the cases with (figure 23) and without (figure 24) the expansion show little difference in the results. The large high entropy regions nearer the shroud reflect the wakes formed by the impeller. However, upon closer inspection, one will note a larger region of increased entropy near the hub wall for the sudden expansion case (figure 23). Obviously, the flowfield is more disturbed in this area. Still, this region is quite small as compared to the impeller exit area. In short, the high entropy zone appears insignificant compared against the sheer size of the impeller exit.

The pseudo-particle traces lead to similar observations. Results for the sudden expansion case are shown in figure 25 while the traces for the case having no excess area are given in figure 26. Note, in both cases, highly tangential streaklines emanate from the suction surface near the shroud. These reflect the classic impeller wake formed by secondary flow.

Subtle differences can observed between the two cases. The sudden expansion case has traces near both walls that appear to

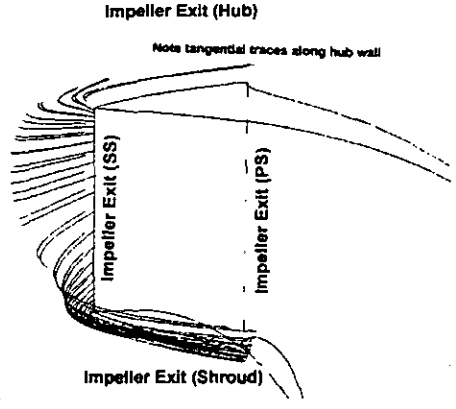

FIGURE 25 – PSEUDO-PARTICLE TRACE WITH SUDDEN EXPANSION

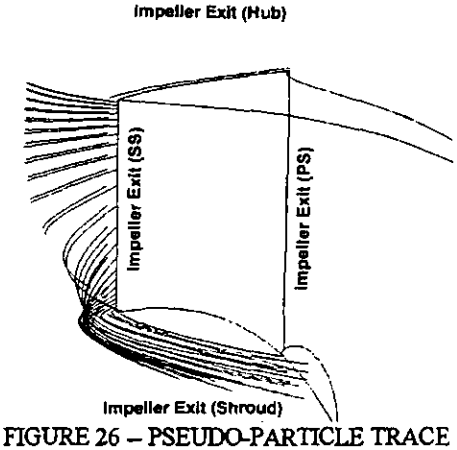

FIGURE 26 – PSEUDO-PARTICLE TRACE WITHOUT SUDDEN EXPANSION

lack radial momentum and remain near the impeller. No such tangential traces appear along the hub wall for the case without the sudden expansion. Also, though not visible in figure 25, the flow within the wake spirals more in the sudden expansion case. Still, the two results do not differ significantly and the area occupied by tangential traces is small compared to the passage area. The bulk of the diffuser passage, in both cases, is dominated by the well-behaved flow, suggesting that the small low momentum regions near the walls will have a lesser effect on the diffuser's effectiveness.

The above CFD results suggest that a large flow coefficient impeller should be less susceptible to the influence of a sudden expansion. These results agree with the findings of Nishida et al. Of course, the high flow case presented herein assumed an area expansion equal to that used for the low flow case. Were the expansion based on the same percentage increase in area, the results would change significantly.

CONCLUSIONS

Many factors determine the applicability of the various diffuser entrance configurations; i.e., operating conditions, rotor deflections, or assembly tolerances. Much work remains before we can totally understand the influences of the diffuser entrance. Additional computational studies; which account for the cover leakage and passage to passage interaction; must be undertaken to determine if leakage flow and exit mixing offset or advance the adverse effects of the excess area. Clearly, a full 360° model and unsteady solution will be required to correctly resolve this complex flow problem.

The results have shown that the Dawes code, BTOB3D, can yield meaningful results despite its limitations. BTOB3D results agreed in principle with the test results published by Kobayashi et al. Therefore, a designer can use the code to search for potential problems with diffuser entrance configurations. The code qualitatively identified detrimental flow phenomena in the diffuser entrance having a sudden expansion.

Based on the CFD results presented and the Kobayashi work, it is evident that inclusion of the extra area promotes diffuser conditions that can lead to premature stall; i.e., zones of depressed static pressure and vortices. The stall can manifest itself as subsynchronous rotor vibrations, a drooping performance curve, pipe vibrations, or other undesirable and potentially harmful consequences. Clearly, the designer must avoid such phenomena and, therefore, should not include excess area above: a) low flow coefficient impellers; b) impellers having a high level of tangential versus radial velocity; and/or c) impellers in any stages in which stall margin is of primary importance. While it may be premature to claim that the large recess area is always problematic, the sudden expansion should only be used after giving careful consideration to impeller exit flow characteristics.

ACKNOWLEDGMENTS

The author wishes to acknowledge Jay Koch, Ed Thierman, and Jim Schufelt, who assisted in the generation of the artwork used herein. I also want to thank Dresser-Rand for allowing me to publish this work.

REFERENCES

1. Casey, M.V., Dalbert, P. and Roth, P., "The Use of 3D Viscous Flow Calculations in the Design and Analysis of Industrial Centrifugal Compressors," ASME paper 90-GT-2 (1990).
2. Dawes, W. N., "Development of a 3D Navier Stokes Solver for Application to all Types of Turbomachinery," ASME paper 88-GT-70 (1988).
3. Jansen, W., "Rotating Stall in a Radial Vaneless Diffuser," Transactions of the ASME - Journal of Basic Engineering, Vol. 86, No. 4, December 1964, pp. 750 - 758.
4. Japikse, D. Turbomachinery Diffuser Design Technology - The Design Technology Series (DTS-1), Concepts, ETI Inc., 1984.
5. Kobayashi, Y., Nishida, H., Takagi, T., and Fukushima, Y., "A Study on the Rotating Stall of Centrifugal Compressors," 2nd Report, "Effect of Vaneless Diffuser Inlet Shape on Rotating Stall," Nippon Kikaigakkai Ronsbunshu (B hen), Vol. 56, No. 529, September 1990, pp. 98 - 103.
6. Kobayashi, Y., Nishida, H., Takagi, T., and Fukushima, Y., "A Study on the Rotating Stall of Centrifugal Compressors," 3rd Report, "Rotating Stall Suppression Method," Nippon Kikaigakkai Ronsbunshu (B hen), Vol. 57, No. 543, November 1991, pp. 3794 - 3800.
7. Kobayashi, Y., Nishida, H., Takagi, T., and Fukushima, Y., "A Study on the Rotating Stall of Centrifugal Compressors," 1st Report, "Effect of Vaneless Diffuser Width on Rotating Stall," Nippon Kikaigakkai Ronsbunshu (B hen), Vol. 54, No. 499, March 1988, pp. 589 - 594.
8. Krain, H., and Hoffman, W., "Verification of an Impeller Design by Laser Measurements and 3D-Viscous Flow Calculations," ASME paper no. 89-GT-159
9. Osborne, C., and Sorokes, J. M., "The Application Of Low Solidity Diffusers in Centrifugal Compressors," Flows In Non-Rotating Turbomachinery Components, ASME FED 69 (1988).
10. Pampreen, R. C., Compressor Surge and Stall, Concepts, ETI, Inc., 1993
11. Senoo, Y., and Kinoshita, Y., "Influence of the Inlet Flow Conditions and Geometries of Centrifugal Vaneless Diffusers on Critical Flow Angle for Reverse Flow," ASME Transactions, Vol. 99, No. 3, Mar. 1977, pp. 98 - 103.
12. Senoo, Y., and Kinoshita, Y., "Limits of Rotating Stall and Stall In Vaneless Diffuser of Centrifugal Compressors," ASME paper 78-GT-19 (1978)
13. Sorokes, J. M., and Welch, J. P., "Experimental Results on a Rotatable Low Solidity Vaned Diffuser," ASME paper 92-GT-19 (1992).